

Hybridization of the amplitude mode in a confined fermionic superfluid

C.R. Cabrera,^{1,2,*} R. Henke,¹ L. Broers,³ J. Skulte,^{2,3} H.P. Ojeda Collado,^{2,3} H. Biss,^{1,2} L. Mathey,^{1,2,3} and H. Moritz^{1,2,†}

¹*Institute for Quantum Physics, Universität Hamburg,
Luruper Chaussee 149, 22761 Hamburg, Germany*

²*The Hamburg Centre for Ultrafast Imaging, Universität Hamburg,
Luruper Chaussee 149, 22761 Hamburg, Germany*

³*Center for Optical Quantum Technologies, Universität Hamburg,
Luruper Chaussee 149, 22761 Hamburg, Germany*

(Dated: July 21, 2025)

In phase transitions, spontaneous symmetry breaking results in a non-zero order parameter and two collective excitations: the Goldstone and the amplitude mode. These modes, which define key properties of superconductors and fermionic superfluids, are well-understood in homogeneous systems. However, their behavior under strong confinement remains largely unexplored, particularly when their excitation energy becomes comparable to the imposed discrete level spacing. In this scenario, hybridization between different collective modes is expected to take place. Here, we show how the amplitude mode hybridizes with a spatial mode in a confined fermionic superfluid. Using lattice modulation spectroscopy, we observe the evolution of the mode throughout the entire crossover from the Bardeen-Cooper-Schrieffer (BCS) state to Bose-Einstein condensation (BEC) of molecules. In the BCS regime, the excitation energy is located at twice the pairing gap, then gradually becomes an in-gap excitation in the strongly correlated regime. Further to the BEC limit, the excitation energy approaches twice the level spacing. The spectral weight of this mode vanishes when approaching the superfluid critical temperature. Our experimental results are in excellent agreement with an effective field theory, providing strong evidence that amplitude oscillations hybridize with and eventually transform into breathing oscillations of the order parameter. The strong modification of the excitation spectrum reveals how confinement and finite-size effects impact fundamental modes of symmetry-broken states.

Bardeen-Cooper-Schrieffer (BCS) theory [1] provides the framework for understanding superconductivity. It describes the formation of Cooper pairs and the emergence of a superconducting energy gap, 2Δ , corresponding to the minimum energy required to break them. However, as P. Anderson noted, significant deviations from this framework can occur in finite-size systems when the characteristic length or energy scale imposed by the confinement approaches the Cooper pair size or the pairing gap energy, respectively [2]. These finite-size effects have been predicted and observed in systems such as nanowires and thin films [3–5], where confinement can modify the dimensionality, enhance the superfluid gap, or increase the critical temperature (T_c), see review [6]. Such phenomena highlight how confinement can be used to engineer superconducting properties.

A key open question we address in this work is how confinement influences the fundamental collective modes of fermionic superfluids and superconductors. These systems are characterized by an order parameter, $\Psi = |\Psi|e^{-i\theta}$, supporting fluctuations in θ and $|\Psi|$, which correspond to the Goldstone mode (gapless phononic excitation) and the amplitude mode (gapped Higgs-like excitation at energy 2Δ), respectively [7, 8]. While these collective modes are well understood in homogeneous sys-

tems, their behavior in the presence of confinement remains largely unexplored. For instance, the excitation spectrum is expected to change qualitatively [9–12], featuring a hybridization of oscillations of the amplitude and the spatial distribution of the order parameter.

In previous work, evidence for amplitude oscillations of the order parameter has been reported in both superconductors [13–16], as well as in ultracold bosonic and fermionic superfluids [17–22]. Additionally, a mesoscopic system has been used to explore precursors of the amplitude mode and its interplay with discrete energy shells [23]. In contrast to these experiments, we study the effect of confinement on the amplitude mode in a macroscopic fermionic superfluid and observe strong evidence of its hybridization with a collective mode of the trap. This is achieved by exploiting the BEC-BCS crossover to tune the pairing gap energy, bringing it close to the trap level spacing. The resulting hybridization is depicted in Fig. 1 a. In the BCS regime, the pairing gap energy is smaller than the trap level spacing. Here, the system exhibits a well-defined resonance with frequency ω_R located at 2Δ (Fig. 1 a, left panel), where the superfluid density $n_s = \int |\Psi|^2 dz$ oscillates in amplitude (red curves). Its frequency coincides with the onset of pair-breaking, however, it is a coherent excitation. Towards the strongly interacting regime, the pairing gap increases, and the amplitude mode hybridizes with the nearest spatial mode of the trap with equal parity, specifically the quantum number $n_z = 2$ (central panel). In this intermediate regime, the resonance energy ω_R drops below 2Δ , and the or-

* cesar.cabrera@physik.uni-hamburg.de

† hennning.moritz@physik.uni-hamburg.de

der parameter acquires a spatially oscillating component, admixing state $n_z = 2$ to the ground state $n_z = 0$. Finally, deep in the BEC regime, the resonance approaches twice the trap level spacing (right panel), resembling a pure breathing mode (blue curves). Our interpretation is based on an effective field theory, which continuously connects the Gross-Pitaevski and Klein-Gordon functionals [7, 24], showing remarkable agreement with our experimental results.

To engineer the mode hybridization, we prepare a homogeneous fermionic superfluid ($T^* < 0.02 T_F$) of ${}^6\text{Li}$ atoms in the lowest two hyperfine states [25, 26]. The system is subjected to strong vertical confinement $\hbar\omega_z = h \cdot 8.7 \text{ kHz}$ (Fig. 1 b), comparable to the Fermi energy $E_F = \hbar^2 4\pi n_{2D}/2m$ [25]. Here, T_F is the Fermi temperature, T^* is the temperature measured after an adiabatic sweep into the BEC regime [25], m is the atom mass, \hbar is the reduced Planck's constant, and n_{2D} is the fermionic density per spin state. To reach the regime where the pairing energy is comparable to the vertical confinement energy, we tune the interaction parameter $\eta = \ln(k_F a_{2D})$ using a Feshbach resonance, where $k_F = \sqrt{4\pi n_{2D}}$ is the Fermi momentum and a_{2D} is the 2D scattering length [27–29]. To probe both spatial and amplitude oscillations of the order parameter, we vary the interaction strength [21, 22] by employing trap modulation spectroscopy [17, 18]. This modulates the harmonic oscillator length l_z and hence the scattering length a_{2D} [25].

Specifically, we modulate the trapping frequency with an amplitude $\alpha \leq 0.5\%$ at a frequency ω_m for a fixed number of periods, $N = 240$, followed by a rethermalization time of 20 ms. To obtain the deposited energy, we adiabatically ramp into the BEC regime ($\eta = -1.7$) and measure the bimodal momentum distribution after time-of-flight (ToF). Here, we extract the condensate amplitude $A(\omega_m)$. This is compared to the condensate amplitude of the unperturbed system $A(0)$, defining our response function $R(\omega_m) = A(0)/A(\omega_m) - 1$ [25]. This normalized function deviates from zero when energy is deposited in the system, revealing resonant frequencies.

In the first series of experiments, we start with a fermionic density of $n_{2D} \approx 1.5 \text{ atoms}/\mu\text{m}^2$, resulting in a ratio of $E_F/\hbar\omega_z = 1.8$. A typical response from trap modulation is shown in the inset of Fig. 2 a. This measurement is extended throughout the entire BEC-BCS crossover in Fig. 2 a, where the color encodes the response $R(\omega_m)$. The vertical axis is normalized to the trapping frequency ω_z , which is independently determined using a fermionic gas with negligible interactions. The system exhibits two distinct excitations. Within the BCS regime, one appears as a broad resonance located at $\omega_m \approx 2\omega_z$, corresponding to single-particle excitations of unpaired atoms to the energy level $n_z = 2$. The other manifests as a narrower resonance at lower frequency, gradually increasing from the BCS ($\eta = 3$) to the BEC ($\eta = -2$) regime, eventually approaching $2\omega_z$.

In the weakly interacting BCS regime, the well-defined resonance is located at nearly twice the pairing gap Δ .

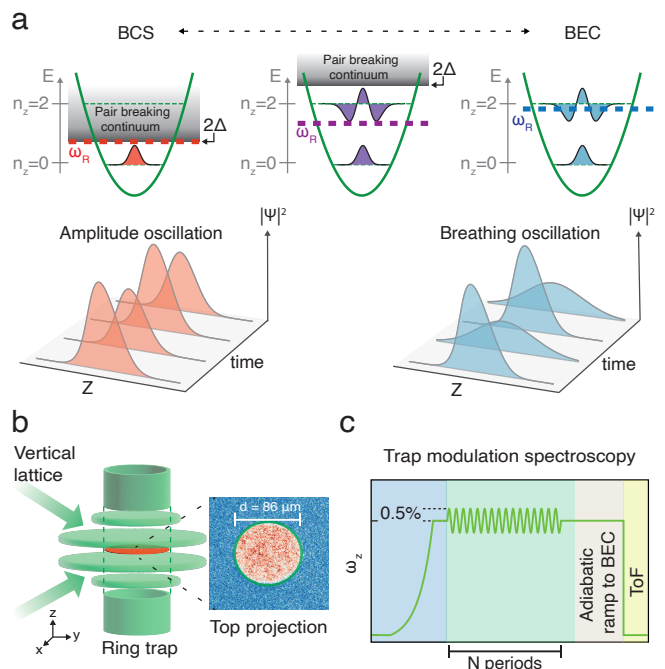


FIG. 1. **a)** Hybridization of amplitude oscillations with spatial excitations. In our confined fermionic superfluid, a well-defined excitation of the order parameter with frequency ω_R is observed throughout the entire BEC-BCS crossover (dashed lines). In the BCS regime, this excitation corresponds to a pure amplitude oscillation of the order parameter located at the onset of the pair-breaking continuum 2Δ . This oscillation conserves the quantum number $n_z = 0$, but the superfluid density $n_s = \int |\Psi|^2 dz$ oscillates in amplitude, illustrated with red curves. In the BEC regime, the excitation at ω_R corresponds to a breathing mode with energy approaching $2\hbar\omega_z$, involving the quantum numbers $n_z = 0$ and $n_z = 2$. This oscillation is sketched with blue curves. In the strongly interacting regime, when Δ becomes comparable to $\hbar\omega_z$, the resulting excitation is a hybridized mode with both breathing and amplitude character. Here, the mode frequency drops below the pair-breaking continuum. **b)** We prepare a homogeneous Fermi gas in a ring-shaped box potential, strongly confined along z with a repulsive lattice potential. The harmonic confinement is comparable to the Fermi energy E_F with $1.5 < E_F/\hbar\omega_z < 2$. **c)** The trapping frequency ω_z is weakly modulated to excite spatial oscillations of the order parameter and amplitude oscillations via the corresponding modulation of the interaction strength. The deposited heat is measured by performing ToF after an adiabatic ramp to the BEC regime.

It agrees with the mean-field prediction of $\Delta = \sqrt{2E_b E_F}$ (red dotted line), where the binding energy E_b is calculated in the 2D limit [25]. This agreement breaks down towards the strongly interacting regime for $\eta < 1.9$, where the observed mode deviates from the onset of the pair-breaking continuum, measured independently via Bragg spectroscopy (red points in Fig. 2 a) [25, 30–33], and instead becomes an in-gap excitation. Finally, in the BEC regime, the order parameter is directly related to the total density and hence only supports spatial os-

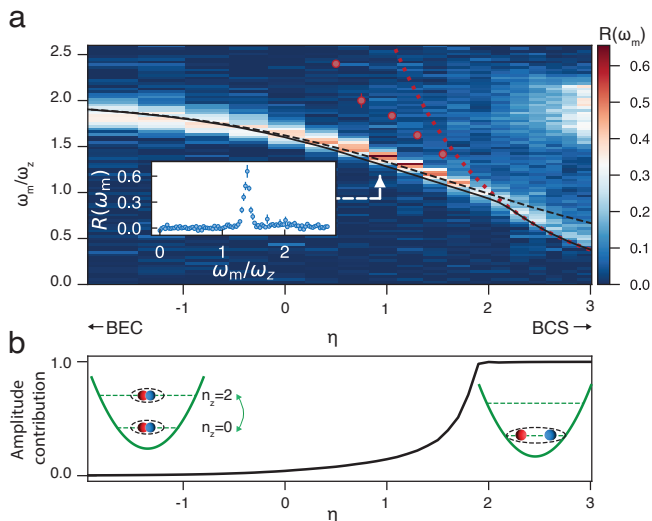


FIG. 2. **a)** Spectral response $R(\omega_m)$ of a confined fermionic superfluid throughout the BEC-BCS crossover, measured via trap modulation spectroscopy. The inset shows a typical response $R(\omega_m)$ for $\eta = 0.97$, with a resonance located below the single-particle excitation energy $2\hbar\omega_z$. In the BCS limit ($\eta \gg 0$), the energy of the resonance agrees with the mean-field value 2Δ (red dotted line). At $\eta = 2$, it deviates from 2Δ , evolving into an in-gap excitation. This is supported by an experimental measurement of 2Δ using Bragg spectroscopy (red points). In the BEC regime ($\eta \ll 0$), where no amplitude mode exists, the excitation corresponds to a breathing mode along the confined direction. Here, its energy is in good agreement with an analytical calculation of the energy difference between the $n_z = 0$ and $n_z = 2$ eigenmodes (black dashed line) extracted from an effective field theory (see main text). The full numerical simulation shows excellent agreement in the entire crossover (black solid line). The error bars show the standard deviation of the mean. **b)** Hybridization of the amplitude mode. For values $\eta > 1.9$, the amplitude character is dominant, quantified by the amplitude contribution extracted from the effective field theory (black line). Here, the excitation does not conserve the total superfluid density, while conserving the quantum number $n_z = 0$. In the BEC regime, the superfluid density is conserved and oscillates spatially involving the $n_z = 2$ eigenmode. In the crossover, the composition of the collective mode corresponds to both amplitude and spatial oscillations of the order parameter.

cillations along the vertical confinement [7]. Here, the resonance corresponds to a breathing excitation of the condensate shifted downwards from $2\hbar\omega_z$ due to repulsive dimer-dimer interactions.

To understand the continuous evolution and character of the resonance, we develop a theoretical model in which the dynamics of the order parameter $\Psi(z, t)$ are described by the equation of motion

$$\begin{aligned}
 & iK_1 \frac{\partial \Psi(z, t)}{\partial t} - K_2 \frac{\partial^2 \Psi(z, t)}{\partial t^2} \\
 & = \left(-\frac{\hbar^2 \partial_z^2}{2M} + V(z, t) - r_0 + u_0 |\Psi(z, t)|^2 \right) \Psi(z, t), \quad (1)
 \end{aligned}$$

derived from a zero-temperature effective field theory [25]. We consider a homogeneous system along the x-y plane and decompose $\Psi(z, t)$ into the $n_z = 0$ and $n_z = 2$ eigenstates of the harmonic potential $V(z, t)$ [25]. In this model, the coefficients K_1 , K_2 , r_0 , and u_0 parameterize the BEC-BCS crossover. These are determined from theoretical predictions for the energy gap, condensate density [34], and speed of sound [35] in the crossover [25]. In the limit where $K_1 = 0$, Eq. 1 reduces to a nonlinear Klein-Gordon equation, describing the order parameter dynamics in the weakly interacting BCS regime. The resulting equation is Lorentz invariant which is a manifestation of particle-hole symmetry. In the BEC limit, where $K_2 = 0$, Eq. 1 reduces to the Gross-Pitaevskii equation.

The black dashed line in Fig. 2 a represents the eigenfrequency difference between the ground and second excited state as analytically obtained from Eq. 1, taking into account interactions to leading order [25]. Towards the BEC regime, this analytical result is in excellent agreement with the experimental observation. The full numerical simulation in the presence of trap modulation (black solid line) extends the agreement throughout the entire BEC-BCS crossover without any fitting parameters. Beyond capturing the mode frequencies, this numerical approach also reveals the composition of the collective excitation due to hybridization, distinguishing between its amplitude and breathing mode components. The theoretical amplitude mode contribution is shown in Fig. 2 b, and represents the fraction of the response where the total superfluid density oscillates in time [25]. In the BCS regime ($\eta \gtrsim 1.9$), this contribution approaches its maximum value, resembling a pure amplitude mode (see red curves in Fig. 1 a). Towards the strongly correlated regime ($\eta \sim 1$), the amplitude mode contribution gradually decreases, and the mode gains breathing character. Finally, in the BEC limit, the dominant excitation is a pure breathing mode, where the superfluid density is constant in time, and oscillates spatially between $n_z = 0$ and $n_z = 2$ (see blue curves in Fig. 1 a).

One feature not captured by our theoretical model is the behavior of the spectral width throughout the crossover, particularly its narrowing in the hybridization regime, which suggests a long-lived and well-defined mode. We quantify the coherence of the mode by computing the quality factor $Q = \omega_0/\delta\omega$, where ω_0 is the resonance frequency and $\delta\omega$ the full width at half maximum extracted from the spectrum. In the entire crossover, the mode remains underdamped with $Q > 0.5$ (Fig. 3 a). Notably, the largest quality factors are found at $\eta < 1.9$, reaching a maximum value in the strongly interacting regime ($\eta \sim 1$). Here, the mode energy is below the onset of the pair-breaking continuum, suggesting that single-particle decay is suppressed, leading to longer lifetimes [10, 36, 37]. This contrasts with a conventional case, where the amplitude mode resides at the onset of the pair-breaking continuum, resulting in strong damping and limited visibility [38–41]. To further confirm the long-lived nature of the mode, we track the free coherent

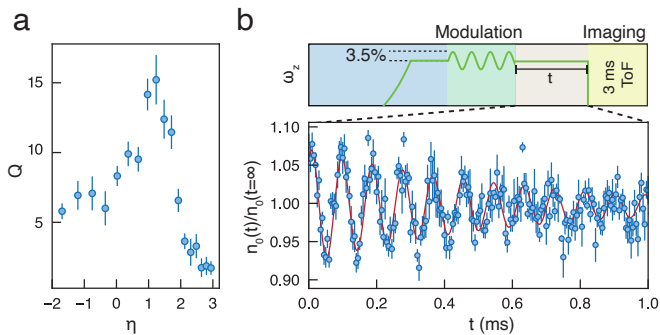


FIG. 3. **a)** Quality factor along the BEC-BCS crossover. We quantify the spectral width via the quality factor Q , extracted from the spectral response in the BEC-BEC crossover. For all interaction strengths we find $Q > 1$, signalling a long-lived excitation throughout the BEC-BCS crossover. The maximum value $Q = 15 \pm 2$ occurs in the strongly correlated regime. **b)** In this regime ($\eta = 1.2$), the collective mode is resonantly excited with a four-period modulation of the trapping frequency. This is followed by a free evolution for a time span t . We observe oscillations of the central density after a ToF expansion of 3 ms. The experimental data is fitted with a damped oscillation yielding a decay time $\tau = (610 \pm 60) \mu\text{s}$ which results in $Q = 21 \pm 2$.

oscillations of the system at $\eta = 1.2$ after a short resonant excitation (Fig. 3 b). We observe a long-lived oscillation at the collective mode frequency ω_0 when measuring the change in the central density of the cloud after 3 ms of ToF [25]. Fitting the data with an exponentially damped oscillation with a decay time τ [25], we obtain a quality factor $Q = \tau\omega_0/2 \approx 21 \pm 2$, comparable with our results from trap modulation spectroscopy.

Since the observed dynamics are compatible with oscillations of the order parameter, we expect a strong temperature dependence, especially close to the superfluid critical temperature T_c . To explore this further, we prepare a strongly interacting system ($\eta = 1.2$) at different temperatures and perform trap modulation spectroscopy [25]. Fig. 4 a shows the spectral response as a function of temperature T^*/T_F . With increasing temperature, the resonance at $2\hbar\omega_z$ associated with single-particle excitations from thermally broken pairs becomes the dominant contribution to the spectrum (see Fig. 4 b). Meanwhile, the collective mode with lower frequency broadens and its spectral weight decreases. The frequency remains constant, resembling the behavior previously observed in Refs. [21, 22, 42]. In Fig. 4 c, the peak amplitude of the mode as a function of temperature is plotted. The observed trend is well described by a bilinear fit, featuring a kink at a temperature of $T_c^* = 0.088(4) T_F$. Remarkably, our previous experiments on the critical velocity in 2D Fermi gases show a critical temperature of $T_c^* = 0.09(2) T_F$ [32]. This supports the interpretation that the collective mode is an excitation of the order parameter which vanishes above a critical temperature.

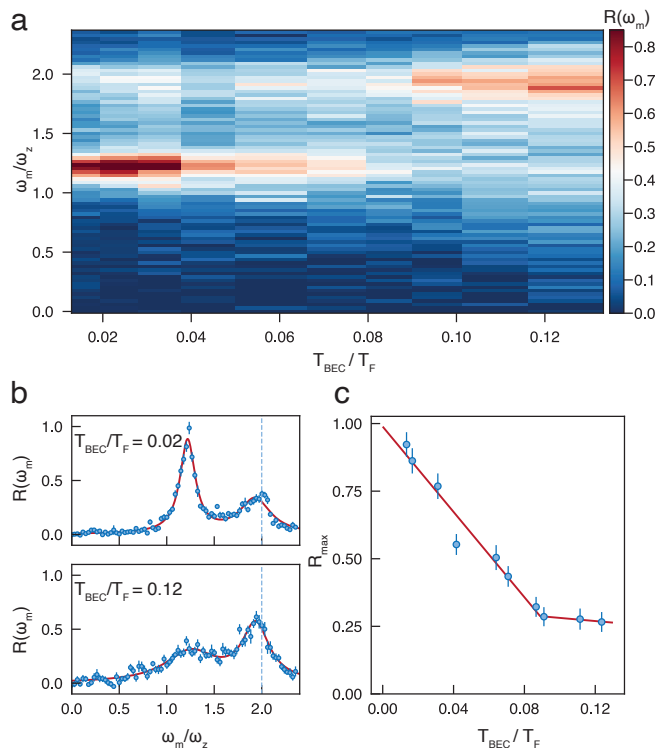


FIG. 4. **a)** Vanishing of the collective mode above the critical temperature. We measure the spectral response $R(\omega_m)$ in the strongly correlated regime ($\eta = 1.2$) as a function of temperature. The collective mode frequency remains nearly constant at $\omega_m/\omega_z \sim 1.2$. As the temperature increases, the mode broadens and its visibility diminishes, signaling the loss of coherence. Above a critical temperature, single-particle transitions at $2\hbar\omega_z$ become the dominant process due to thermally broken pairs. **b)** To extract the critical temperature, we fit the maximum response of the collective mode R_{max} by a double Lorentzian function (red line) shown for two vertical cuts of panel a. **c)** The temperature dependence of the maximum response shows a kink, which we identify as the critical temperature T_c^* . Employing a bilinear fit (red line), we obtain $T_c^* = 0.088(4) T_F$.

In conclusion, our study focuses on a fundamental feature of strongly confined fermionic superfluids: the hybridization of collective modes. We observe a well-defined resonance in the entire BEC-BCS crossover, which we interpret as an excitation of the order parameter. This interpretation is supported by the strong suppression of the resonance above the critical temperature and the excellent agreement with the effective field theory.

Additionally, we show that trap modulation spectroscopy is a powerful tool for determining the pairing gap in the BCS regime and the superfluid-to-normal transition in the crossover. This is of interest for studying spin-imbalanced superfluids and other strongly correlated 2D systems.

Beyond ultracold atoms, these results provide insights into the hybridization of modes in confined fermionic superfluids and superconductors, such as low-dimensional

materials and nano-superconducting devices. Here, the hybridization could influence fundamental properties such as the critical velocity or critical temperature. Our work paves the way to investigate more complex dynamics of the order parameter under confinement [43, 44], such as frequency beating [45], drum modes [18], exotic Higgs bound states [46, 47] or Leggett modes [48–50]. Finally, it is an exciting prospect to use confinement to control the properties of many-body systems by admixing higher harmonic oscillator states [51, 52].

Acknowledgements. We gratefully acknowledge fruitful discussions with Y. Castin, T. Enss, D. Jaksch, J. Leonard, J. Levinsen, T. Lompe, M. Parish, P. Pieri and M. Zwierlein. This work is supported by the Deutsche Forschungsgemeinschaft (DFG, German Research Foundation) in the framework of SFB-925—project 170620586—and the Cluster of Excellence “CUI: Advanced Imaging of Matter”—EXC

2056—project ID 390715994 and co-financed by ERDF of the European Union and by “Fonds of the Hamburg Ministry of Science, Research, Equalities and Districts (BWFGB)”.

Author Contributions. R.H., H.B. and C.R.C. performed the experiments and analysed the data. L.B., J.S. and H.P.O.C. developed the theoretical model and numerical simulations. L.M. and H.M. supervised the work. All authors contributed extensively to the interpretation of the results and to the preparation of the manuscript.

Data availability. The datasets supporting this study are available from the corresponding authors upon request.

Competing interests. The authors declare no competing interests.

Correspondence and requests for materials should be addressed to C. R. Cabrera or H. Moritz.

-
- [1] J. Bardeen, L. N. Cooper, and J. R. Schrieffer, Theory of superconductivity, *Phys. Rev.* **108**, 1175 (1957).
- [2] P. W. Anderson, Theory of dirty superconductors, *J. Phys. Chem. Solids* **11**, 26 (1959).
- [3] J. M. Blatt and C. J. Thompson, Shape resonances in superconducting thin films, *Phys. Rev. Lett.* **10**, 332 (1963).
- [4] A. A. Shanenko, M. D. Croitoru, M. Zgirski, F. M. Peeters, and K. Arutyunov, Size-dependent enhancement of superconductivity in al and sn nanowires: Shape-resonance effect, *Phys. Rev. B* **74**, 052502 (2006).
- [5] B. Abeles, R. W. Cohen, and G. W. Cullen, Enhancement of superconductivity in metal films, *Phys. Rev. Lett.* **17**, 632 (1966).
- [6] S. Bose and P. Ayyub, A review of finite size effects in quasi-zero dimensional superconductors, *Rep. Prog. Phys.* **77**, 116503 (2014).
- [7] D. Pekker and C. M. Varma, Amplitude/Higgs modes in condensed matter physics, *Annu. Rev. Condens. Matter Phys.* **6**, 269 (2015).
- [8] R. Shimano and N. Tsuji, Higgs mode in superconductors, *Annu. Rev. Condens. Matter Phys.* **11**, 103 (2020).
- [9] A. Korolyuk, J. J. Kinnunen, and P. Törmä, Density response of a trapped Fermi gas: A crossover from the pair vibration mode to the Goldstone mode, *Phys. Rev. A* **84**, 033623 (2011).
- [10] A. Korolyuk, J. J. Kinnunen, and P. Törmä, Collective excitations of a trapped Fermi gas at finite temperature, *Phys. Rev. A* **89**, 013602 (2014).
- [11] J. Hertkorn, F. Böttcher, M. Guo, J. N. Schmidt, T. Langen, H. P. Büchler, and T. Pfau, Fate of the amplitude mode in a trapped dipolar supersolid, *Phys. Rev. Lett.* **123**, 193002 (2019).
- [12] J. Bjerlin, S. M. Reimann, and G. M. Bruun, Few-Body precursor of the higgs mode in a fermi gas, *Phys. Rev. Lett.* **116**, 155302 (2016).
- [13] R. Sooryakumar and M. V. Klein, Raman scattering by superconducting-gap excitations and their coupling to charge-density waves, *Phys. Rev. Lett.* **45**, 660 (1980).
- [14] R. Matsunaga, N. Tsuji, H. Fujita, A. Sugioka, K. Makise, Y. Uzawa, H. Terai, Z. Wang, H. Aoki, and R. Shimano, Light-induced collective pseudospin precession resonating with Higgs mode in a superconductor, *Science* **345**, 1145 (2014).
- [15] M.-A. Méasson, Y. Gallais, M. Cazayous, B. Clair, P. Rodière, L. Cario, and A. Sacuto, Amplitude Higgs mode in the 2H-NbSe₂ superconductor, *Phys. Rev. B* **89**, 060503 (2014).
- [16] D. Sherman, U. S. Pracht, B. Gorshunov, S. Poran, J. Jesudasan, M. Chand, P. Raychaudhuri, M. Swanson, N. Trivedi, A. Auerbach, M. Scheffler, A. Frydman, and M. Dressel, The Higgs mode in disordered superconductors close to a quantum phase transition, *Nat. Phys.* **11**, 188 (2015).
- [17] U. Bissbort, S. Götze, Y. Li, J. Heinze, J. S. Krauser, M. Weinberg, C. Becker, K. Sengstock, and W. Hofstetter, Detecting the amplitude mode of strongly interacting lattice bosons by Bragg scattering, *Phys. Rev. Lett.* **106**, 205303 (2011).
- [18] M. Endres, T. Fukuhara, D. Pekker, M. Cheneau, P. Schauss, C. Gross, E. Demler, S. Kuhr, and I. Bloch, The ‘Higgs’ amplitude mode at the two-dimensional superfluid/Mott insulator transition, *Nature* **487**, 454 (2012).
- [19] J. Léonard, A. Morales, P. Zupancic, T. Donner, and T. Esslinger, Monitoring and manipulating Higgs and Goldstone modes in a supersolid quantum gas, *Science* **358**, 1415 (2017).
- [20] A. Behrle, T. Harrison, J. Kombe, K. Gao, M. Link, J.-S. Bernier, C. Kollath, and M. Köhl, Higgs mode in a strongly interacting fermionic superfluid, *Nat. Phys.* **14**, 781 (2018).
- [21] P. Dyke, S. Musolino, H. Kurkjian, D. J. M. Ahmed-Braun, A. Pennings, I. Herrera, S. Hoinka, S. J. J. M. F. Kokkelmans, V. E. Colussi, and C. J. Vale, Higgs oscillations in a unitary Fermi superfluid, *Phys. Rev. Lett.* **132**, 223402 (2024).
- [22] A. Kell, M. Breyer, D. Eberz, and M. Köhl, Exciting the higgs mode in a strongly interacting fermi gas by interaction modulation, *Phys. Rev. Lett.* **133**, 150403 (2024).

- [23] L. Bayha, M. Holten, R. Klemt, K. Subramanian, J. Bjerlin, S. M. Reimann, G. M. Bruun, P. M. Preiss, and S. Jochim, Observing the emergence of a quantum phase transition shell by shell, *Nature* **587**, 583 (2020).
- [24] J. Skulte, L. Broers, J. G. Cosme, and L. Mathey, Vortex and soliton dynamics in particle-hole-symmetric superfluids, *Phys. Rev. Res.* **3**, 043109 (2021).
- [25] See Supplemental Material.
- [26] K. Hueck, N. Luick, L. Sobirey, J. Siegl, T. Lompe, and H. Moritz, Two-dimensional homogeneous Fermi gases, *Phys. Rev. Lett.* **120**, 060402 (2018).
- [27] D. S. Petrov and G. V. Shlyapnikov, Interatomic collisions in a tightly confined Bose gas, *Phys. Rev. A* **64**, 012706 (2001).
- [28] J. Levinsen and M. M. Parish, Strongly interacting two-dimensional Fermi gases, *Annual Review of Cold Atoms and Molecules*, **3**, 1 (2015).
- [29] A. V. Turlapov and M. Yu Kagan, Fermi-to-Bose crossover in a trapped quasi-2d gas of fermionic atoms, *J. Phys. Condens. Matter* **29**, 383004 (2017).
- [30] G. Veeravalli, E. Kuhnle, P. Dyke, and C. J. Vale, Bragg spectroscopy of a strongly interacting Fermi gas, *Phys. Rev. Lett.* **101**, 250403 (2008).
- [31] S. Hoinka, P. Dyke, M. G. Lingham, J. J. Kinnunen, G. M. Bruun, and C. J. Vale, Goldstone mode and pair-breaking excitations in atomic Fermi superfluids, *Nat. Phys.* **13**, 943 (2017).
- [32] L. Sobirey, N. Luick, M. Bohlen, H. Biss, H. Moritz, and T. Lompe, Observation of superfluidity in a strongly correlated two-dimensional Fermi gas (2021).
- [33] H. Biss, L. Sobirey, N. Luick, M. Bohlen, J. J. Kinnunen, G. M. Bruun, T. Lompe, and H. Moritz, Excitation spectrum and superfluid gap of an ultracold Fermi gas, *Phys. Rev. Lett.* **128**, 100401 (2022).
- [34] L. Salasnich, Condensate fraction of a two-dimensional attractive Fermi gas, *Phys. Rev. A* **76**, 015601 (2007).
- [35] H. Shi, S. Chiesa, and S. Zhang, Ground-state properties of strongly interacting Fermi gases in two dimensions, *Phys. Rev. A* **92**, 033603 (2015).
- [36] R. Verresen, R. Moessner, and F. Pollmann, Avoided quasiparticle decay from strong quantum interactions, *Nat. Phys.* **15**, 750 (2019).
- [37] J. Lorenzana and G. Seibold, Long-lived Higgs modes in strongly correlated condensates, *Phys. Rev. Lett.* **132**, 026501 (2024).
- [38] T. Cea, C. Castellani, G. Seibold, and L. Benfatto, Non-relativistic dynamics of the amplitude (Higgs) mode in superconductors, *Phys. Rev. Lett.* **115**, 157002 (2015).
- [39] T. Cea, C. Castellani, and L. Benfatto, Nonlinear optical effects and third-harmonic generation in superconductors: Cooper pairs versus Higgs mode contribution, *Phys. Rev. B* **93**, 180507 (2016).
- [40] H. Kurkjian, S. N. Klimin, J. Tempere, and Y. Castin, Pair-breaking collective branch in BCS superconductors and superfluid Fermi gases, *Phys. Rev. Lett.* **122**, 093403 (2019).
- [41] H. Kurkjian, J. Tempere, and S. N. Klimin, Linear response of a superfluid fermi gas inside its pair-breaking continuum, *Sci. Rep.* **10**, 11591 (2020).
- [42] C. Vaswani, J. H. Kang, M. Mootz, L. Luo, X. Yang, C. Sundahl, D. Cheng, C. Huang, R. H. J. Kim, Z. Liu, Y. G. Collantes, E. E. Hellstrom, I. E. Perakis, C. B. Eom, and J. Wang, Light quantum control of persisting Higgs modes in iron-based superconductors, *Nat. Commun.* **12**, 258 (2021).
- [43] S. Hannibal, P. Kettmann, M. D. Croitoru, A. Vagov, V. M. Axt, and T. Kuhn, Quench dynamics of an ultracold Fermi gas in the BCS regime: Spectral properties and confinement-induced breakdown of the Higgs mode, *Phys. Rev. A* **91**, 043630 (2015).
- [44] S. Hannibal, P. Kettmann, M. D. Croitoru, V. M. Axt, and T. Kuhn, Dynamical vanishing of the order parameter in a confined bardeen-cooper-schrieffer Fermi gas after an interaction quench, *Phys. Rev. A* **97**, 013619 (2018).
- [45] H. P. O. Collado, N. Defenu, and J. Lorenzana, Engineering Higgs dynamics by spectral singularities, *Phys. Rev. Res.* **5**, 023011 (2023).
- [46] T. Nakayama, I. Danshita, T. Nikuni, and S. Tsuchiya, Fano resonance through Higgs bound states in tunneling of Nambu-Goldstone modes, *Phys. Rev. A* **92**, 043610 (2015).
- [47] T. Nakayama and S. Tsuchiya, Perfect transmission of Higgs modes via antibound states, *Phys. Rev. A* **100**, 063612 (2019).
- [48] A. J. Leggett, Number-phase fluctuations in two-band superconductors, *Progress of Theoretical Physics* **36**, 901 (1966).
- [49] H. Krull, N. Bittner, G. S. Uhrig, D. Manske, and A. P. Schnyder, Coupling of Higgs and Leggett modes in non-equilibrium superconductors, *Nature Communications* **7**, 11921 (2016).
- [50] F. Giorgianni, T. Cea, C. Vicario, C. P. Hauri, W. K. Withanage, X. Xi, and L. Benfatto, Leggett mode controlled by light pulses, *Nature Physics* **15**, 341 (2019).
- [51] K. G. Jackson, C. J. Dale, J. Maki, K. G. S. Xie, B. A. Olsen, D. J. M. Ahmed-Braun, S. Zhang, and J. H. Thywissen, Emergent *s*-wave interactions between identical fermions in quasi-one-dimensional geometries, *Phys. Rev. X* **13**, 021013 (2023).
- [52] C. J. Dale, K. G. S. Xie, K. Pond Grehan, S. Zhang, J. Maki, and J. H. Thywissen, Emergent *s*-wave interactions in orbitally active quasi-two-dimensional fermi gases, *Phys. Rev. A* **110**, L051302 (2024).
- [53] T. C. Li, H. Kelkar, D. Medellin, and M. G. Raizen, Real-time control of the periodicity of a standing wave: an optical accordion, *Opt. Express* **16**, 5465 (2008).
- [54] S. Al-Assam, R. A. Williams, and C. J. Foot, Ultracold atoms in an optical lattice with dynamically variable periodicity, *Phys. Rev. A* **82**, 021604 (2010).
- [55] J. L. Ville, T. Bienaimé, R. Saint-Jalm, L. Corman, M. Aidelsburger, L. Chomaz, K. Kleinlein, D. Perconte, S. Nascimbène, J. Dalibard, and J. Beugnon, Loading and compression of a single two-dimensional Bose gas in an optical accordion, *Phys. Rev. A* **95**, 013632 (2017).
- [56] A. M. Fischer and M. M. Parish, BCS-BEC crossover in a quasi-two-dimensional fermi gas, *Phys. Rev. A* **88**, 023612 (2013).
- [57] J. Zhou, T. Shi, X.-J. Liu, H. Hu, and W. Zhang, BCS-BEC crossover in a quasi-two-dimensional fermi superfluid, *New J. Phys.* **25**, 083001 (2023).
- [58] P. Dyke, K. Fenech, T. Peppler, M. G. Lingham, S. Hoinka, W. Zhang, S.-G. Peng, B. Mulkerin, H. Hu, X.-J. Liu, and C. J. Vale, Criteria for two-dimensional kinematics in an interacting Fermi gas, *Phys. Rev. A* **93**, 011603 (2016).

- [59] M. Cyrot, Ginzburg-landau theory for superconductors, Reports on Progress in Physics **36**, 103 (1973).

Supplementary Material: Hybridization of the amplitude mode in a confined fermionic superfluid

I. PREPARATION

A. Box potential

We prepare a homogeneous Fermi gas of ${}^6\text{Li}$ atoms in the lowest two hyperfine states $|1\rangle$ and $|2\rangle$. A Feshbach resonance located at 832 G allows to control the interaction strength. The confinement in the xy -plane is provided by a radial repulsive optical ring potential with diameter $d = 86 \mu\text{m}$ [26]. In the vertical direction, the gas is strongly confined to a single layer of a blue-detuned lattice potential with tunable spacing ($20 \mu\text{m} - 3 \mu\text{m}$) [53–55]. This results in trapping frequencies of up to $\omega_z = 2\pi \cdot 12 \text{ kHz}$.

A typical density is $n_{2D} \approx 1.5 \text{ atoms}/\mu\text{m}^2$, corresponding to a Fermi energy $E_F \approx h \cdot 15 \text{ kHz}$ and Fermi temperature $T_F \approx 700 \text{ nK}$. The lowest temperature in our system is $T^* \approx 20 \text{ nK} \approx 0.014 T_F$, which is extracted from a wing fit of the non-condensed fraction after T/4 time-of-flight (ToF) expansion in the BEC regime ($B = 750 \text{ G}$). This system is the starting point for the experiments presented in the main text, whose parameters are summarized in Tab. I.

B. 2D Parametrization

In our experiments, the Fermi energy E_F is comparable to the trap level spacing $\hbar\omega_z$. This motivates our parametrization of the system in terms of pure 2D quantities using the column density n_{2D} , 2D Fermi energy $E_F = \hbar^2 k_F^2 / 2m$, Fermi momentum $k_F = \sqrt{4\pi n_{2D}}$, and the atom mass m .

In the presence of strong confinement the quasi-2D scattering amplitude is given by

$$f_{\text{quasi},2D}(k, a_{3D}, l_z) = \frac{4\pi}{\sqrt{2\pi} l_z / a_{3D} + w(k^2 l_z^2 / 2)}, \quad (2)$$

with the 3D scattering length a_{3D} , the harmonic oscillator length $l_z = \sqrt{\hbar / (m\omega_z)}$ and the momentum-dependent contributions to the scattering amplitude $w(x)$ [27]. In the low-momentum limit $kl_z \rightarrow 0$, the quasi-2D scattering amplitude simplifies to

$$f_{\text{quasi},2D,0}(k, a_{3D}, l_z) = \frac{4\pi}{\sqrt{2\pi} l_z / a_{3D} - \ln\left(\frac{2\pi k^2 l_z^2}{A}\right) + i\pi} \quad (3)$$

with $A \approx 0.915$. Comparing the pure 2D scattering amplitude with the simplified quasi-2D scattering amplitude

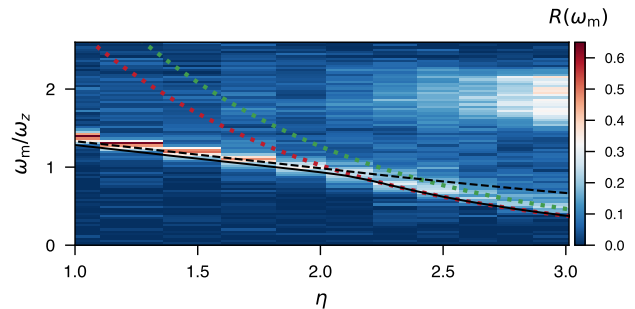


FIG. S1. Comparison of the spectrum shown in Fig. 2 in the BCS regime with the 2D pairing gap (red dashed) and pairing gap taking the vertical confinement into account (Eq. 6, green dashed). In addition, the resonance positions from the effective field theory are shown (black dashed and black dashed lines, see Fig. 2).

in Eq. 3 it is possible to obtain a relation between the 2D scattering length and the 3D scattering length,

$$a_{2D} = l_z \sqrt{\frac{\pi}{A}} e^{-\sqrt{\frac{\pi}{2}} l_z / a_{3D}} \quad (4)$$

The 2D scattering length is used in the main text to define the interaction strength $\eta = \ln(k_F a_{2D})$ and the mean-field pairing gap

$$\Delta = \sqrt{2E_b E_F} \quad (5)$$

with the binding energy of the 2D bound state $E_b = \hbar^2 / (ma_{2D}^2)$. This parametrization enables us to compare the experimental data with the prediction from an effective field theory, whose free parameters are constrained by existing mean-field and Quantum Monte Carlo calculations. For more details, see Section III.

We note that beyond mean-field effects as well as the occupation of excited states along the confined direction can lead to modifications of Δ [56, 57]. When considering only the lowest two harmonic states $n = 0, 1$, an analytical expression is given by [56]

$$\frac{\Delta}{E_F} \simeq \sqrt{\frac{2E_b}{E_F}} \left(1 + \frac{E_F}{8\omega_z}\right), \quad (6)$$

which we plot in Fig. S1 (green dashed line).

The figure suggest that taking into account the occupation of higher levels should improve the agreement of the effective field theory with the experimental data. As accurate predictions for speed of sound are not available for our ratio of E_F / ω_z , we choose to consistently use purely 2D predictions, where QMC calculations are available.

Fig.	avg.	n [$1/\mu\text{m}^2$]	$\omega_F/2\pi$ [kHz]	$\omega_z/2\pi$ [kHz]	ω_F/ω_Z
2 A & 3 A (ω_z -mod)	10	1.54 ± 0.07	16.2 ± 0.4	8.57 ± 0.5	1.89 ± 0.11
2 A (onset 2Δ)	20	1.19 ± 0.05	12.5 ± 0.6	6.15 ± 0.04	2.03 ± 0.02
3 B (oscillations)	5	1.46 ± 0.14	15.4 ± 1.4	8.57 ± 0.5	1.80 ± 0.11
4 (T -dependence)	15	1.35 ± 0.04	14.3 ± 0.4	11.46 ± 0.33	1.25 ± 0.04

TABLE I. Number of averages, densities, Fermi energies and trapping frequencies for the measurements displayed in the referenced figures.

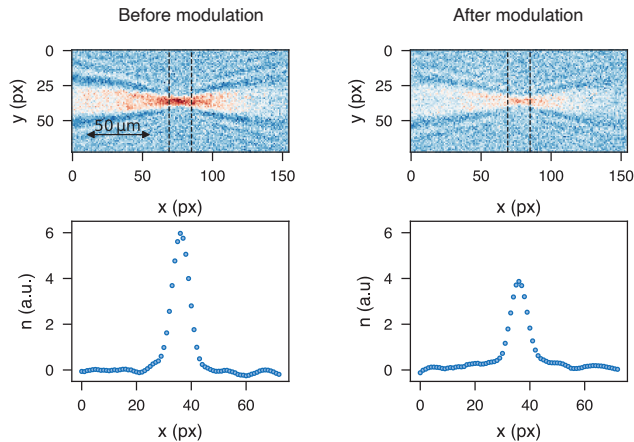


FIG. S2. Momentum distribution after trap modulation is acquired by expanding the gas in an in-plane harmonic trap for a quarter trap period. Due to the strong vertical confinement, the gas expands rapidly out of the depth of field of the high-resolution microscope. Therefore, we tilt the imaging axis, to map the z -position to the x -axis and extract the in-focus part (region within black dashed lines). The in-focus momentum distributions shows a clear condensate peak. Its reduction allows for the extraction of the deposited heat during modulation.

II. PROBING

A. Response measurement

Trap modulation spectroscopy is performed after creating a strongly confined and homogeneous system. At a given interaction strength η , the trapping frequency is modulated by 0.5% at a given frequency ω_m (see Fig. 1c in the main text). This scheme allows a deposition of energy into the system when being resonant with a mode, resulting in an increase of temperature and subsequent reduction of the condensate fraction after a rethermalization time of 20 ms.

In order to extract the response, the reduction in the condensate amplitude $A(\omega_m)$ from the bimodal momentum distribution is used. We define the response as $R(\omega_m) = A(0)/A(\omega_m) - 1$, which is a proxy for the deposited heat into the system [33]. The amplitude $A(\omega_m)$ is extracted by mapping to momentum space via a ToF expansion for a quarter period in an in-plane harmonic potential [26]. Due to the strong vertical confinement, the cloud simultaneously expands rapidly along z , such

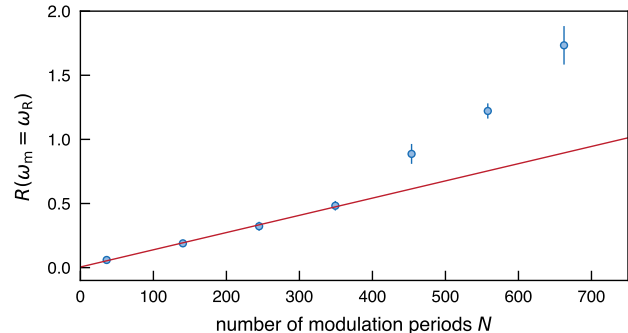


FIG. S3. The response of modulation spectroscopy for varying number of modulation periods N . The response increases linearly up to a $N = 350$ modulation periods, shown by linear fit taking the first four points into account. For these measurements a modulation amplitude $\alpha = 1\%$ and frequency $\omega_m = 18$ kHz is used.

that it becomes larger than the depth of field of the high-resolution microscope. Therefore, we tilt the imaging beam with respect to the optical axis of the imaging system. This projects the z -position onto the x -axis, which allows us to extract the in-focus momentum distribution (Fig. S2) with a horizontal average over the central region within the black-dashed lines. To obtain the condensate peak height, we perform a moving average of 8 px over the momentum distribution and then take the peak density $A_i(\omega_m)$. For each modulation frequency ω_m , we take multiple images, extract the peak densities $A_i(\omega_m)$ and average them to $A(\omega_m)$.

To ensure linear response, we drive the system on resonance (18 kHz at 900 G) for different numbers of modulation periods N and extract the response, shown in Fig. S3. The response behaves linearly up to $N = 350$ oscillation periods. We want to stay well below this point and therefore fix the modulation periods to $N = 240$ for $\omega_m > 2$ kHz. Below 2 kHz, we keep the modulation time at $240/2$ kHz = 120 ms, to avoid diverging probe times when going to low frequencies. All resonances we observe via trap modulation are well above 2 kHz.

B. Oscillation Measurement

The measurements of the time dynamics presented in Fig. 3b in the main text use a similar protocol pre-

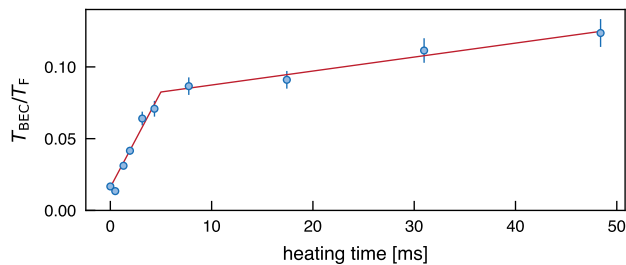


FIG. S4. Temperature T^* of the atomic cloud measured in the BEC regime. We employ Bragg spectroscopy to locally heat up the system for different driving time. An empirical bilinear fit (red line) is used to obtain a calibration from heating time to temperature.

sented in section II A. Here, the system is excited with a short modulation of only two oscillation periods, see inset Fig. 3 b, with a large modulation amplitude of $\alpha = 3.5\%$. Afterwards, the system evolves freely for different times t , where the occupation of the $n_z = 2$ harmonic oscillator state periodically oscillates. When the vertical confinement is suddenly removed, the excess of transverse kinetic energy due to the partial population of the $n_z = 2$ state results in a rapid expansion along z leading to a larger transverse cloud width and a rapid decrease in the central density of the cloud. The time evolution of the central density is detected after a short ToF of 3 ms. A similar technique has been used in Ref. [58] to measure the transverse excitations in quasi-2D Fermi gases. We fit the observed oscillations with an exponential decay $n_0(t) \propto \sin(\omega_0 t + \phi_0)e^{-t/\tau}$ with decay time τ and phase ϕ_0 . From the fitted decay time we obtain the quality factor $Q = \tau\omega_0/2$.

C. Temperature dependence

To investigate the temperature effects on the order parameter presented in Fig. 4 in the main text, we heat up the system by exciting the phonon mode at low momentum via Bragg spectroscopy ($q = 0.48 k_F$). After a variable heating time followed by a fixed time for rethermalisation, we are able to have full control of the temperature of the system. The temperature, defined as T^* in the main text is calibrated by performing a wing fit to the momentum distribution acquired after T/4 ToF measurement in the BEC regime ($B = 750$ G and $\eta = -1.7$) [26]. The temperature T^* as a function of driving time is shown in Fig. S4. To accurately extract the temperature from the thermal wings, each point is averaged over 50 measurements. We use an empirical bilinear fit (red line), to translate the heating times to the temperatures presented in Fig. 4 in the main text. For the largest temperature of $T^*/T_F \sim 0.12$, the thermal excitations are still below the first excited state due to confinement ($\hbar\omega_z/k_B T^* > 6$).

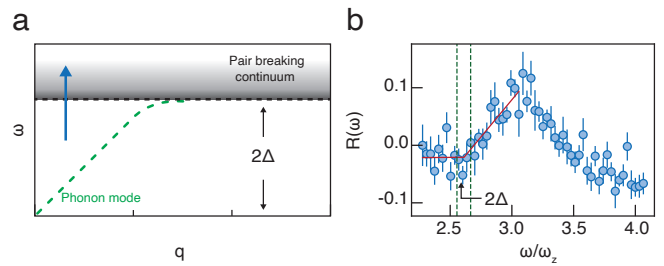


FIG. S5. **a)** Sketch of the excitation spectrum of a fermionic superfluid in the BCS regime. The phononic Bogoliubov mode (dashed green) with the typical linear dispersion relation at low momentum q merges into the pair-breaking continuum (gray area) which is gapped by 2Δ . The blue arrow indicates the regime where Bragg spectroscopy is performed to extract the pairing gap. **b)** Experimental measurement of the pairing gap using Bragg spectroscopy at momentum $q = 0.48 k_F$. The position of the onset is extracted from a bilinear fit (red line). It is shown with its corresponding uncertainty in position (green dashed lines).

D. Extraction of the pair-breaking continuum

To compare the position of the gap with respect to the order parameter oscillations, we perform Bragg spectroscopy with low in-plane momentum $q = 0.48 k_F$ (dashed line in Fig. S5 a). For Fig. 2 in the main text, we determine the size of the pairing gap by finding the onset of the pair-breaking continuum (red points) located at 2Δ . The spectral response of the onset is shown in Fig. S5 b (blue points). The gap is extracted from the intersection point of a bilinear fit (red line).

III. EFFECTIVE FIELD THEORY

To gain further insights, we model the system using a low-energy effective field theory [7, 24] describing the dynamics of a complex-valued bosonic scalar field Ψ which represents the condensed pairs. To be able to capture both, the BCS- and BEC-dynamics, we include a dynamical term in the form of $K_2 |\partial_t \Psi(\mathbf{r}, t)|^2$ to model particle-hole symmetric dynamics and a term of the form of $iK_1 \Psi^*(\mathbf{r}, t) \partial_t \Psi(\mathbf{r}, t)$ to include non-particle-hole symmetric dynamics. The parameters K_1 and K_2 control the influence of both terms and are determined by the underlying system as discussed later. The action can be written as

$$\mathcal{S} = \mathcal{S}_{\text{dyn}} + \mathcal{S}_{\text{stat}} \equiv \int dt \mathcal{L}. \quad (7)$$

We use the following action and Lagrangian in the form of

$$\mathcal{S}_{\text{dyn}} = \int d^3 r dt \left(iK_1 (\Psi(\mathbf{r}, t) \partial_t \Psi^*(\mathbf{r}, t) - \text{c.c.}) + K_2 |\partial_t \Psi(\mathbf{r}, t)|^2 \right) \quad (8)$$

$$\mathcal{S}_{\text{stat}} = \int d^3r dt \left(-r_0 |\Psi(\mathbf{r}, t)|^2 + \frac{u_0}{2} |\Psi(\mathbf{r}, t)|^4 + \frac{\hbar^2}{2M} |\nabla \Psi(\mathbf{r}, t)|^2 \right) \quad (9)$$

where the parameters K_1 and K_2 interpolate between particle-hole symmetric and non particle-hole symmetric dynamics, r_0 is a bias with the character of a chemical potential and u_0 is the density-density interaction strength. The precise values of these parameters have to be determined for different values of η throughout the crossover. We note that the static part only contains standard terms included in Ginzburg-Landau theory [59].

Due to the second time derivative, the total particle number is not conserved as we can see from the Noether charge, which is given by

$$J = i \int d^3r [\Pi(r, t)\Psi(r, t) - \Pi(r, t)^*\Psi(r, t)^*] \quad (10)$$

with the canonical conjugate defined as

$$\Pi(r, t) = \frac{\partial \mathcal{L}}{\partial(\partial_t \Psi(r, t))} = K_2 \partial_t \Psi^*(r, t) - iK_1 \Psi^*(r, t). \quad (11)$$

A. Determination of the free parameters

In order to extract predictions from the effective field theory, the values of our free parameters $K_{1/2}$, u_0 , M and r_0 have to be determined throughout the entire BEC-BCS crossover. We use the following constraints: As the complex scalar field describes the bosonic Cooper pair

wavefunction, we set $M = 2m$. We will further consider that during the crossover the energy scale has to be fixed. This enforces a constraint on the sum of K_1 and K_2 . To recover the GPE limit for $K_2 = 0$ and the BCS limit for $K_1 = 0$ we choose

$$K_1 = \hbar - 2K_2 E_F / \hbar. \quad (12)$$

Next, we identify the amplitude and Goldstone mode in our effective model in the absence of confinement. For this we invoke the Euler-Lagrange equations to obtain

$$\begin{aligned} \partial_t (-K_2 \partial_t + iK_1) \Psi(r, t) = \\ (-r_0 - \frac{\hbar^2}{2M} \nabla^2 + u_0 |\Psi(r, t)|^2) \Psi(r, t). \end{aligned} \quad (13)$$

We obtain the steady state solution by setting all time derivatives to zero and find $|\Psi_0|^2 = \frac{r_0}{u_0}$. Next, we expand our complex field around the fixed point to lowest order

$$\Psi = \Psi_0 + \delta_a + i\Psi_0 \phi \equiv \Psi_0 + \delta_a + i\delta_\phi, \quad (14)$$

where we used the underlying $U(1)$ symmetry to choose the phase of the fixed point to be zero. We expand the complex field in Eq. 14, keeping only the lowest order. By taking the Fourier transform and separating the real and imaginary part we obtain

$$K_2 \omega^2 \delta_a - i\omega K_1 \delta_\phi = 2r_0 \delta_a + \frac{\hbar^2}{2M} q^2 \delta_a \quad (15)$$

$$K_2 \omega^2 \delta_\phi + i\omega K_1 \delta_a = \frac{\hbar^2}{2M} q^2 \delta_\phi, \quad (16)$$

where ω is the frequency and q the momentum. Solving for ω , we obtain

$$\omega_\phi = \sqrt{\frac{K_1^2 + 2K_2 \left(\frac{\hbar^2}{2M} q^2 + r_0 \right) - \sqrt{K_1^4 + 4K_2^2 r_0^2 + 4K_1^2 K_2 \left(\frac{\hbar^2}{2M} q^2 + r_0 \right)}}{2K_2^2}} \quad (17)$$

$$\omega_a = \sqrt{\frac{K_1^2 + 2K_2 \left(\frac{\hbar^2}{2M} q^2 + r_0 \right) + \sqrt{K_1^4 + 4K_2^2 r_0^2 + 4K_1^2 K_2 \left(\frac{\hbar^2}{2M} q^2 + r_0 \right)}}{2K_2^2}}, \quad (18)$$

where ω_a denotes the amplitude mode and ω_ϕ the Goldstone mode. For the special case $K_1 = 0$, corresponding to particle-hole symmetry, we recover the well-known result, that the modes decouple [7] and are given by

$$\omega_{\phi, K_1=0} = \sqrt{\frac{\hbar^2}{2MK_2}} |q| \quad (19)$$

$$\omega_{a, K_1=0} = \sqrt{\frac{2r_0 + \frac{\hbar^2}{2M} q^2}{K_2}}. \quad (20)$$

Taking the limit of $K_2 \rightarrow 0$ in Eq. 17 recovers the Bogoliubov dispersion relation with $K_1 = \hbar$ and $r_0 = \mu$

$$\hbar\omega = \sqrt{\left(\frac{\hbar^2 q^2}{2M} \right)^2 + 2\mu \frac{\hbar^2 q^2}{2M}}. \quad (21)$$

To determine the remaining free parameters, we use the condensate density n_0 in the 2D BEC-BCS crossover, which we take from [34]. For the amplitude mode energy 2Δ , we take the 2D mean-field result (Eq. 5). Additionally, we consider the speed of sound v_s as reported from

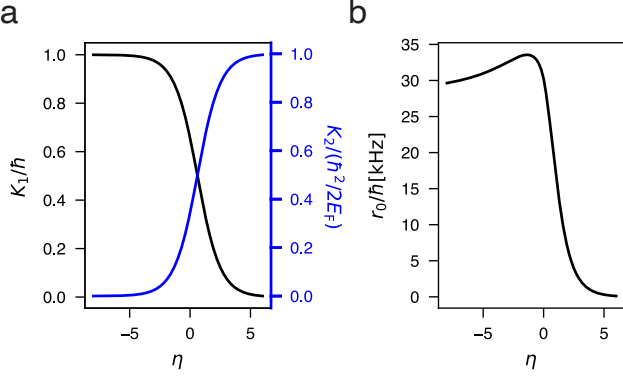


FIG. S6. The effective parameters in the crossover. **a)** K_1 in units of \hbar and K_2 in units of $\hbar^2/(2E_F)$ and **b)** r_0 in units of \hbar kHz. Not shown is u_0 that can be simply computed by r_0/n_0 and follows a similar trend as r_0 . As η flips sign a rapid change in parameters can be observed.

previous work using 2D Quantum Monte Carlo [35]. In our model these quantities relate to each other as

$$n_0 = r_0/u_0 \quad (22)$$

$$v_s = \left. \frac{\partial \omega_a}{\partial q} \right|_{q=0} = \hbar^2 \sqrt{\frac{r_0}{M}} \sqrt{\frac{1}{(\hbar^2 - 2E_F K_2)^2 + 2\hbar^2 K_2 r_0}} \quad (23)$$

$$2\Delta = \hbar \omega_a \Big|_{q=0} = \sqrt{\frac{2(\hbar - \frac{2E_F K_2}{\hbar})^2 + 4K_2 r_0}{2K_2^2}}, \quad (24)$$

thereby fixing the remaining free parameters in our effective low-energy model, r_0 , u_0 , K_1 and K_2 (using Eq. 12). Fig. S6 depicts these parameters between $\eta = -8$ and $\eta = 6$ during the crossover. We find that for $\eta < -4$ we recover the expected broken particle-hole symmetry of a BEC, hence $K_2 \approx 0$ and $K_1 \approx \hbar$. On the BCS side we find that $K_2 \approx \hbar^2/2E_F$ and $K_1 \approx 0$.

B. Effective two-mode model

After fixing the parameters by considering a 2-dimensional condensate, we introduce a strong spatial confinement along the z direction analogous to the experiment and expand the wavefunction to find a simplified two-mode model that we use for our numerical results in the main text. We also carry out numerics including the full z -dynamics and quantitatively find the same results. For simplicity, and as it allows a direct interpretation of the emerging mode, we have chosen to present the two-mode model here and in the main text.

We start by rewriting the complex scalar field as

$$\Psi(x, y, z) = \Phi(x, y)\Phi(z). \quad (25)$$

Since the experiment uses a box potential, we assume that there are no spatial modulations along the $x - y$ direction and expand the field as uniform in this plane. Along the z direction, we have a strong harmonic confinement, meaning the atoms only occupy the harmonic oscillator ground state. Assuming that our effective u_0 is small and only acts as a perturbation to the harmonic oscillator ground state and assuming we only access the lowest eigenstates, we expand the complex scalar field as

$$\Psi(x, y, z) = \frac{1}{L_x L_y} [f_0(z)\alpha_0 + f_1(z)\alpha_1 + f_2(z)\alpha_2] \quad (26)$$

with the harmonic oscillator (HO) eigenfunctions

$$f_n(z) = \frac{1}{\sqrt{2^n n!}} \left(\frac{1}{l_{z,M} \sqrt{\pi}} \right)^{\frac{1}{2}} e^{-\frac{M\omega_z}{2\hbar} z^2} H\left(n, \frac{z}{l_{z,M}}\right) \quad (27)$$

with the harmonic oscillator length $l_{z,M} = \sqrt{\hbar/(M\omega_z)}$ and n -th Hermite polynomial $H(n, z)$. Due to the driving in the experiment, the system can couple to higher states. However, due to parity symmetry, our drive does not couple to the first, but to the second excited state. By construction, integration over the $x - y$ direction leads to unity. We checked numerically that the first level of the HO is always empty during the dynamics and we neglect this contribution in the following, reducing our system to the ground and second excited state. Next, we use this expansion to compute the integrals in Eq. 9 and Eq. 8, from which we obtain

$$\begin{aligned} \int d^3r \Psi^*(x, y, z) \left[-r_0 + \frac{u_0}{2} \Psi^*(x, y, z) \Psi(x, y, z) \right] \Psi(x, y, z) = & -r_0(\alpha_0^* \alpha_0 + \alpha_2^* \alpha_2) \\ & + \frac{u_0}{2} \frac{1}{16} \sqrt{\frac{M\omega_z}{\pi\hbar}} \left[12\sqrt{2}\alpha_2^* \alpha_0^* \alpha_2 \alpha_0 + 8\sqrt{2}\alpha_0^* \alpha_0^* \alpha_0 \alpha_0 + \frac{41}{8}\sqrt{2}\alpha_2^* \alpha_2^* \alpha_2 \alpha_2 \right] \\ & + \frac{u_0}{2} \frac{1}{16} \sqrt{\frac{M\omega_z}{\pi\hbar}} \left[(-8\alpha_0^* \alpha_0^* \alpha_2 \alpha_0 + \alpha_2^* \alpha_2^* \alpha_2 \alpha_0 + 3\sqrt{2}\alpha_2^* \alpha_2^* \alpha_0 \alpha_0) + \text{h.c.} \right]. \end{aligned} \quad (28)$$

From the driven HO contribution, we further assume $\omega_z(t)^2 = \omega_z^2 + a(t)$ and $a(t) = b\omega_z^2 \sin(\omega_m t)$. We compute

$$\begin{aligned} & \int d^3r \Psi^*(x, y, z) \left[-\frac{\hbar^2}{2M} \partial_z^2 + \frac{1}{2} M (\omega_z^2 + a(t)) z^2 \right] \Psi(x, y, z) \\ &= \frac{\hbar\omega_z}{2} \left(\alpha_0^* \alpha_0 + 5\alpha_2^* \alpha_2 + \frac{b(t)}{2} \left[\alpha_0^* \alpha_0 + 5\alpha_2^* \alpha_2 + \frac{\sqrt{2}}{2} (\alpha_2^* \alpha_0 + \alpha_0^* \alpha_2) \right] \right), \end{aligned} \quad (29)$$

with the short hand notation $a(t) = b\omega_z^2 \sin(\omega_m t) = b(t)\omega_z^2$. Finally, for the dynamical part of the Lagrangian we obtain

$$\int d^3r \mathcal{L}_{\text{dyn}} = -K_2 (\partial_t \alpha_0 \partial_t \alpha_0^* + \partial_t \alpha_2 \partial_t \alpha_2^*) + iK_1 \{ (\alpha_0^* \partial_t \alpha_0 - \alpha_0 \partial_t \alpha_0^*) + (\alpha_2^* \partial_t \alpha_2 - \alpha_2 \partial_t \alpha_2^*) \}. \quad (30)$$

Invoking the Euler-Lagrange equations then leads to the equations of motion:

$$\partial_t (-K_2 \partial_t + iK_1) \alpha_0 = \left(-\tilde{r}_0 + \frac{\hbar\omega_z}{2} [1 + b(t)] \right) \alpha_0 + b(t) \frac{\sqrt{2}\hbar\omega_z}{4} \alpha_2 \quad (31)$$

$$+ \frac{u_0}{2} \frac{1}{16} \sqrt{\frac{M\omega_z}{\pi\hbar}} \left[12\sqrt{2}\alpha_2^* \alpha_2 \alpha_0 + 16\sqrt{2}\alpha_0^* \alpha_0 \alpha_0 - 16\alpha_0^* \alpha_2 \alpha_0 - 8\alpha_2^* \alpha_0 \alpha_0 + \alpha_2^* \alpha_2 \alpha_2 + 6\sqrt{2}\alpha_0^* \alpha_2 \alpha_2 \right]$$

$$\partial_t (-K_2 \partial_t + iK_1) \alpha_2 = \left(-\tilde{r}_0 + 5\frac{\hbar\omega_z}{2} [1 + b(t)] \right) \alpha_2 + b(t) \frac{\sqrt{2}\hbar\omega_z}{4} \alpha_0 \quad (32)$$

$$+ \frac{u_0}{2} \frac{1}{16} \sqrt{\frac{M\omega_z}{\pi\hbar}} \left[12\sqrt{2}\alpha_0^* \alpha_2 \alpha_0 + \frac{41}{4} \sqrt{2}\alpha_2^* \alpha_2 \alpha_2 - 8\alpha_0^* \alpha_0 \alpha_0 + 2\alpha_2^* \alpha_2 \alpha_0 + \alpha_0^* \alpha_2 \alpha_2 + 6\sqrt{2}\alpha_2^* \alpha_0 \alpha_0 \right].$$

C. Numerical results

We study the linear response of the system to the trap modulation $b(t)$. To obtain the black solid line of Fig. 2 a in the main text, we proceed as follows. We choose a driving amplitude $b = 0.01$, which is small enough to ensure that we are probing the linear feedback of the system. We further add a small dissipation term in the form of $-\hbar\gamma\partial_t\Psi(z, t)$ in the left-hand side of Eq.31-32 to allow the system to reach a steady state. In the simulation we take $\gamma = 10^{-2}$. We numerically solve the order parameter dynamics $\Psi(t)$ following Eq.31-32 and extract the Fourier component of $\Delta n(t) = n(t) - n(0)$ at the driving frequency ω_m

$$\Delta n(\omega_m) = \int_{t_0}^{t_0+\Delta t} \Delta n(t) \exp(i\omega_m t) dt \quad (33)$$

where $n(z, t) = \sum_{i=0,2} |\alpha_i|^2$ is the field density. After the system reaches a steady state at time t_0 , we consider a time window $\Delta t = 50T_z$ ($T_z = 2\pi/\omega_z$) which is sufficient to obtain a good frequency resolution.

Finally we compute the response function $\Delta n(\omega_m) = \int |\Delta n(z, \omega_m)| dz$ for different modulation frequencies ω_m and extract the frequency ω_c at which the response takes the maximum value. This frequency ω_c give us the corresponding collective mode. Doing this for different interaction parameters $\eta = \ln(k_F a_{2D})$, we obtain the collective mode dependence on η which is depicted by a black solid line in Fig. 2 a of the main text.

To quantify the amplitude contribution to the collective mode, we define

$$\kappa_A = \frac{|\int \Delta n(z, \omega_c) dz|}{\int |\Delta n(z, \omega_c)| dz}, \quad (34)$$

representing the fraction of the total response, which does not conserve the integrated field density. Following this definition, far in the BEC regime the integral in the numerator vanishes, so $\kappa_A = 0$ and the collective mode has a pure breathing contribution. This is because in the BEC regime, the order parameter response is simply redistributed along the z direction in a way that the field density remains constant, resulting in a vanishing numerator after integrating over space. Conversely, in the BCS regime, the order parameter dynamics is dominated by amplitude oscillations, i.e. the integrated field density changes, and the numerator does not vanish. In this case, the collective mode shows an amplitude contribution ($\kappa_A > 0$). We compute the amplitude contribution κ_A numerically as a function of η which is plotted in Fig. 2 b of the main text.

D. Analytical results

Here we derive the analytical solution for the transition frequency $\Delta\omega = \omega_2 - \omega_0$ between the ground and second excited state shown as a dashed black line in Fig. 2 a of the main text.

For this we compute the collective modes associated to the bosonic system described by Eqs. 31,32 by keeping only the leading order interacting terms, i.e. considering $\alpha_2 \sim 0$ and $\alpha_0^* \alpha_0 = (r_0 - \omega_z K_1/2)/u_0$ in the terms proportional to u_0 . By collecting terms proportional to α_0 in Eq. 31 and proportional to α_2 in Eq. 32 the equations of motion simplify to:

$$\partial_t (-K_2 \partial_t + iK_1) \alpha_0 = \left(-\tilde{r}_0 + \frac{\hbar\omega_z}{2} + \delta_0 \right) \alpha_0, \quad (35)$$

$$\partial_t (-K_2 \partial_t + iK_1) \alpha_2 = \left(-\tilde{r}_0 + 5\frac{\hbar\omega_z}{2} + \delta_2 \right) \alpha_2, \quad (36)$$

with the last terms on the right hand side of both equations representing a correction to the energy (mean-field shift) due to interactions. They are given by:

$$\delta_0 = \frac{\sqrt{2}}{2} \sqrt{\frac{M\omega_z}{\pi\hbar}} (r_0 - \omega_z K_1/2) \quad (37)$$

$$\delta_2 = \frac{12\sqrt{2}}{32} \sqrt{\frac{M\omega_z}{\pi\hbar}} (r_0 - \omega_z K_1/2). \quad (38)$$

The collective modes associated to the resulting equations of motion (34) and (35) can be obtained by introducing an ansatz of the type $\alpha_n \sim \exp(i\omega_n t)$. This yields

$$\omega_n^\pm = \frac{-K_1}{2K_2} \pm \sqrt{\frac{K_1^2}{4K_2^2} + \frac{E_n}{K_2}} \quad (39)$$

with $E_n = \hbar\omega_z(n + \frac{1}{2}) - \tilde{r}_0 + \delta_n$ and $n = 0, 2$. Finally, we define $\Delta\omega = \omega_2^+ - \omega_0^+ = -(\omega_2^- - \omega_0^-)$.